

Highlights

General CAV platoon considering the time-varying communication delay: system modeling and stability

Tiancheng Ruan,Hao Wang,Zewen Zuo,Gengyue han,Beier Ba,Changyin Dong

- A generic supermatrix modeling approach for the CAV platoon considering time-varying communication delay is proposed.
- A novel stability condition of the CAV platoon considering the time-varying delay is derived based on Lyapunov-Krasovskii Stability Theorem.
- The Wirtinger-Based Integral Inequality is adopted instead of the Jensen inequality to derive a more accurate stability condition.
- A comprehensive evaluation analysis of the tracking performance and safety conditions for different control parameters and IFTs is performed under various scenarios.

General CAV platoon considering the time-varying communication delay: system modeling and stability

Tiancheng Ruan^{a,b,c}, Hao Wang^{a,b,c,*}, Zewen Zuo^{a,b,c}, Gengyue han^{a,b,c}, Beier Ba^{a,b,c} and Changyin Dong^{a,b,c}

^aJiangsu Key Laboratory of Urban ITS, Southeast University, 2 Si Pai Lou, Nanjing, 210096, P.R. China

^bJiangsu Province Collaborative Innovation Center of Modern Urban Traffic Technologies, 2 Si Pai Lou, Nanjing, 210096, P.R. China

^cSchool of Transportation, Southeast University, 2 Si Pai Lou, Nanjing, 210096, P.R. China

ARTICLE INFO

Keywords:

Connected Automated Vehicle (CAV)
CAV platoon
Stability analysis
Time-varying communication delay
Tracking performance

ABSTRACT

Driven by the potential of connected autonomous vehicles (CAVs), recent research has focused on their benefits on safety, emissions, and capability. These benefits are preconditioned on the satisfaction of stability, the primary goal of CAVs. However, due to the unavoidable communication delay, stability cannot be absolutely guaranteed by the widely adopted feedback control. Therefore, numerous research has been conducted to derive stability conditions considering communication delay. However, limited by the adopted methodology, most of the research implicitly assumes that the communication delay is set as a constant representing the maximum communication delay. The fact is that communication delay is time-varying according to the variation of the surrounding environment. In general, there is a lack of a method for deriving the stability conditions considering the time-varying delay. Therefore, to address this problem, this paper first proposes a generic supermatrix modeling approach for the CAV platoon considering time-varying communication delay. Moreover, a novel stability condition considering the time-varying delay of the generic CAV platoon is derived by applying Wirtinger-Based Integral Inequality and the Lyapunov-Krasovskii Stability Theorem. Furthermore, extensive numerical analyses in various scenarios are conducted to comprehensively evaluate the tracking performance and safety conditions of different control parameters and information flow topologies (IFTs) and thus shed some light. The results indicate that all CAVs under different control parameters and IFTs have smooth tracking performance if stability is guaranteed. In addition, increasing the gain of spacing and velocity errors can benefit tracking performance and safety conditions, while increasing the gain of acceleration errors does not. Moreover, Leader-based and bi-directional communication enables superior tracking and transient performance.

1. Introduction

Since the automobile was invented over a century ago, automotive engineers have been dedicated to delivering safer and more comfortable service. However, traffic problems such as traffic congestion, accidents, and pollutant emissions have become more prominent in recent decades (Schrank et al., 2019; Jin and Orosz, 2016; Ruan et al., 2022). For these problems, traditional traffic engineers have adopted external measures like traffic management and traffic control to improve them. Nevertheless, these external measures are increasingly ineffective and gradually face bottlenecks. Through the research of static and dynamic characteristics of traffic flow, the heterogeneity of human factors is regarded as the main cause of this phenomenon (Zhong et al., 2020; van Arem et al., 2016; Ye and Yamamoto, 2018; Ruan et al., 2021).

Benefiting from technology development, Automated Vehicle (AV) stands out as a promising enabler and has gained significant popularity in academia and the automotive industry in recent years. It measures the state error relative to the predecessor through on-board sensing devices to enable tracking. Due to its simplicity and effectiveness, it becomes increasingly available as standard equipment in modern commercial vehicles with the market penetration rate (MPR) increasing (Wilson and Ward, 2011; Wilson, 2008). Consequently, much research on AV has revealed its superiority over human vehicles in capacity, safety, and emissions (Góñi-Ros et al., 2019; Nikolos et al., 2015; Kesting et al., 2010).

*Corresponding author

✉ ruantiancheng@seu.edu.cn (T. Ruan); haowang@seu.edu.cn (H. Wang); 220203312@seu.edu.cn (Z. Zuo); gyhan@seu.edu.cn (G. han); 980794728@qq.com (B. Ba); dongcy@seu.edu.cn (C. Dong)

ORCID(s):

However, AVs are restricted by access to information and, therefore, cannot fully utilize the potential of autonomous driving. Thanks to the development of Cellular vehicle-to-everything (C-V2X) and wireless communication technology, Connected Automated Vehicle (CAV) emerged. Armed with Vehicle-to-Infrastructure (V2I) / Vehicle-to-Vehicle (V2V) communication, CAVs can acquire information more accurately with less delay, even beyond the sight (Navas and Milanés, 2019; Zhou et al., 2021). Moreover, CAVs have the potential to implement more elaborate platoon control strategies relative to AVs (Dey et al., 2015; Zheng et al., 2015a). This enables the CAV platoon to achieve system optimization rather than user optimization to leverage further the safety and capacity gains of CAV (Ghiasi et al., 2017; Li et al., 2020). At present, extensive research has been conducted on CAVs, including the exploration of the gain on capacity (Sala and Soriguera, 2021; Chang et al., 2020), safety (Zhou et al., 2019; Montanino and Punzo, 2021; Yu et al., 2021), and pollutant emission (Liu et al., 2018; Xiao et al., 2018).

Despite the advantages mentioned above of the CAVs, this is all based on the prerequisite of satisfying stability, which is the primary goal of the CAVs. Specifically, the transient response caused by perturbation fades with time. However, due to the unavoidable communication delay, stability cannot be absolutely guaranteed by the widely adopted feedback control. Therefore, extensive research has been conducted to derive stability conditions considering delay (Herman et al., 1959; Zhang and Jarrett, 1997; Li et al., 2010, 2013; Kamath et al., 2015; Sun et al., 2018). Herman et al. (Herman et al., 1959) adopted the Laplace transform based method for a simple linear time-delay model and obtained its characteristic equation. Then the stability conditions were obtained through numerical methods. On this basis, Zhang and Jarrett (Zhang and Jarrett, 1997) also used the Laplace transform based method to develop a linear time-delay model for the product of the sensitivity and the reaction time. In addition, a more general and analytic stability condition is obtained by a characteristic equation-based approach. Furthermore, Li et al. (Li et al., 2010, 2013) took the full velocity difference car-following model as an example to derive the stability condition using second Lyapunov method, and the corresponding simulation was carried out to investigate the effect of different parameters on the dynamic performance of the traffic flow. Kamath et al. (Kamath et al., 2015) linearized the classical car-following model and the optimal velocity model to construct the characteristic equation considering the reaction delay. Then the Nyquist stability criterion is employed to obtain the corresponding stability conditions. Moreover, Sun et al. (Sun et al., 2018) comprehensively reviewed major methods for analyzing the stability of the time-delay car-following model and verified the consistency and applicability of some of the stability conditions by numerical simulations.

Although the above stability analysis methods can effectively derive stability conditions considering the communication delay, most have an unrealistic assumption that the communication delay is set as a constant representing the maximum communication delay, limited by the fundamental methodology adopted. In practice, however, the communication delay is time-varying according to the variation of the surrounding environment. This is because the basic methodology of the aforementioned methods can be divided mainly into methods based on the frequency domain and methods based on the second Lyapunov method. The frequency domain-based methods are difficult to deal with the high dimensionality present in time-varying time-delay systems since the time-varying delay turns ordinary differential equations into delay-differential equations, which are infinite dimensional systems and difficult to be solved analytically (Lhachemi and Prieur, 2020). While second Lyapunov method-based methods need to be generalized to the functional space when dealing with time-varying time delays, which leads to additional constraints for different trajectories, thus resulting in conservativeness of the obtained stability conditions due to approximations and additional constraints (Fridman, 2006; Wang et al., 2016; Lian et al., 2020). Therefore, to derive stability conditions for CAV considering time-varying delay, a stability analysis method capable of handling time-varying delay needs to be developed to obtain more accurate stability conditions.

Thus, this paper proposes a generic supermatrix modeling approach for the CAV platoon considering the time-varying communication delay. Moreover, a novel stability condition of the generic CAV platoon considering the time-varying delay is derived by applying the Wirtinger-Based Integral Inequality and Lyapunov-Krasovskii Stability Theorem. To sum up, the main contributions of this paper can be divided into three aspects:

1. A generic supermatrix modeling approach for the CAV platoon considering time-varying communication delay is proposed.
2. A novel stability condition of the CAV platoon is derived considering the time-varying delay under the general representation proposed based on Lyapunov-Krasovskii Stability Theorem.
3. The Wirtinger-Based Integral Inequality is adopted instead of the Jensen inequality to derive a more accurate stability condition.
4. Extensive numerical analyses in various scenarios are conducted to comprehensively evaluate the tracking performance and safety conditions of different control parameters and thus provide guidance for the selection.

The remainder of the paper is outlined as follows: Section 2 introduces the mathematical preliminaries, including graph theory and two essential integral inequalities. Section 3 presents the supermatrix modeling approach of the CAV platoon considering time-varying communication delay and a corresponding general representation. Corresponding stability analyses and the derivation of stability conditions based on the Lyapunov-Krasovskii Stability Theorem are carried out in Section 4. Moreover, Section 5 proposes a comprehensive performance evaluation analysis of the different control parameters on tracking performance and safety conditions. We summarize the paper in Section 6.

Notations: Throughout the paper \mathbb{R}^n denotes the n-dimensional Euclidean space with Euclidian norm $|\cdot|$ while the set of all $m \times n$ real matrices is denoted by $\mathbb{R}^{m \times n}$. The sets \mathbb{S}_n and \mathbb{S}_n^+ mean the set of symmetric and symmetric positive definite matrices of $\mathbb{R}^{n \times n}$, respectively. Moreover, $p_i(t)$, $v_i(t) = \dot{p}_i(t)$, $a_i(t) = \ddot{p}_i(t)$, and $\dot{a}_i(t) = \dddot{p}_i(t) \in \mathbb{R}$ denote the longitudinal position, speed, acceleration, and jerk of vehicle i at time t , respectively. The transpose of a vector or a matrix A is denoted by A^T . The symmetric matrix $\begin{bmatrix} A & B \\ * & C \end{bmatrix}$ denotes $\begin{bmatrix} A & B \\ B^T & C \end{bmatrix}$. Besides, for any square matrix $A \in \mathbb{R}^{n \times n}$, we define $He(A) = A + A^T$. I_n defines the identity matrix of $n \times n$ dimension while $0_{m,n}$ stands for the zero matrix of $m \times n$ dimension. For any matrix $A \in \mathbb{R}^{n \times n}$, the notation $A > 0$ denotes that A is symmetric and positive definite. The set of continuous functions from an interval $[-h, 0] \subset \mathbb{R}$ to \mathbb{R}^n which are, consequently, square integrable is denoted as Banach space $C([-h, 0], \mathbb{R}^n)$. For any function $f \in C$, the uniform norm $|f|_h$ refers to

$$\sup_{\theta \in [-h, 0]} |f(\theta)|. diag \{a_1, a_2, \dots, a_n\}$$
 stands for the diagonal matrix $\begin{bmatrix} a_1 & 0 & 0 \\ 0 & \ddots & 0 \\ 0 & 0 & a_n \end{bmatrix}$ whose diagonal elements starting at the upper left corner are a_1, a_2, \dots, a_n .

Let $A \in \mathbb{R}^{m \times n}$ and $B \in \mathbb{R}^{p \times q}$, then $A \otimes B$ is the Kronecker product of A and B :

$$A \otimes B = \begin{bmatrix} a_{11}B & \cdots & a_{1n}B \\ \vdots & \ddots & \vdots \\ a_{m1}B & \cdots & a_{mn}B \end{bmatrix} \in \mathbb{R}^{mp \times nq}.$$

Let $C \in \mathbb{R}^{m \times n}$ and $D \in \mathbb{R}^{m \times n}$, then $C \circ D$ is the Hadamard product of C and D :

$$C \circ D = \begin{bmatrix} c_{11}d_{11} & \cdots & c_{1n}d_{1n} \\ \vdots & \ddots & \vdots \\ c_{m1}d_{m1} & \cdots & c_{mn}d_{mn} \end{bmatrix} \in \mathbb{R}^{m \times n}.$$

2. Preliminaries

2.1. Network model

By regarding each vehicle in the platoon as a node and intervehicle communication as an edge, the information flow topology (IFT) among the platoon can be modeled as a weighted directed graph (digraph) $\mathcal{G} = \{\mathcal{V}, \mathcal{E}, \mathcal{A}\}$, in which $\mathcal{V} = \{1, 2, \dots, n\}$ is the set of nodes and $\mathcal{E} \subseteq \mathcal{V} \times \mathcal{V}$ is the set of edges. Besides, the weighted adjacent matrix with nonnegative elements is defined as $\mathcal{A} = [a_{ij}]_{n \times n}$ with $a_{ii} = 0$ which denotes that the self-edges (i, i) is not allowed unless indicated otherwise. The edge (i, j) in \mathcal{E} means the vehicle i can communicate with vehicle j associated with weighted a_{ij} . Defining the degree matrix of \mathcal{G} as $\mathcal{D} = diag \{d_1, d_2, \dots, d_n\}$, with $d_i = \sum_{j \in \mathcal{V}} a_{ij}$. Therefore, the Laplacian matrix \mathcal{L} of the weighted digraph \mathcal{G} can be defined as $\mathcal{L} = \mathcal{D} - \mathcal{A}$.

2.2. Integral inequality

Integral inequalities provide sufficient help for the study of lower bounds of quadratic function integrals in the stability analysis of state delayed systems (Martyniuk and Gutovski, 1979; Zhang et al., 2016; Li et al., 2021). Wirtinger Integral inequalities, being one of them, are considered to be effective and less conservative (Saravanan et al., 2021; Suresh and Manivannan, 2021). Wirtinger Integral inequalities are a series of integral inequalities that estimate the integral of the derivative function based on the integral of the function. The Wirtinger Integral inequality adopted here is stated below:

Lemma 1 (Wirtinger Integral Inequality) (Park et al., 2015). Consider a given $n \times n$ matrix $R > 0$. Then, for all function z in $C([-h, 0], \mathbb{R}^n)$ which satisfies $z(-h) = z(0) = 0$, the following inequality holds:

$$\int_{-h}^0 \dot{z}^T(u) R \dot{z}(u) du \geq \frac{\pi^2}{h^2} \int_{-h}^0 z^T(u) R z(u) du. \quad (1)$$

Note that although Jensen inequality (Gu et al., 2003) is applied in most research to determine the lower bounds of quadratic function integrals, its inclusion of inherent conservatism makes the results less accurate. A more accurate lower bound can be obtained by Wirtinger Integral Inequality, as shown in Remark 6.

Moreover, another useful lemma inspired by the reciprocally convex combination is introduced below:

Lemma 2 (Park et al., 2011). For given positive integers n, m , assume a scalar α in the interval $(0, 1)$, a given $n \times n$ matrix $R > 0$ and two matrices W_1 and W_2 in $\mathbb{R}^{n \times m}$. For all vector ξ in \mathbb{R}^m , the function $\Theta(\alpha, R)$ is given by:

$$\Theta(\alpha, R) = \frac{1}{\alpha} \xi^T W_1^T R W_1 \xi + \frac{1}{1-\alpha} \xi^T W_2^T R W_2 \xi. \quad (2)$$

Then, if there exists a matrix X in $\mathbb{R}^{n \times n}$ such that $\begin{bmatrix} R & X \\ * & R \end{bmatrix} > 0$, then the following inequality holds:

$$\min_{\alpha \in (0,1)} \Theta(\alpha, R) \geq \begin{bmatrix} W_1 \xi \\ W_2 \xi \end{bmatrix}^T \begin{bmatrix} R & X \\ * & R \end{bmatrix} \begin{bmatrix} W_1 \xi \\ W_2 \xi \end{bmatrix}. \quad (3)$$

3. System modeling

Consider a group of n CAVs moving along a single lane and forming a CAV platoon where the intra-vehicle communication functions according to the IFT. Fig. 1 shows the schematic of the CAV platoon with typical four IFTs: Predecessor-Follower (PF), (b) Predecessor-Leader-Follower (PLF), (c) Bi-Directional (BD), and (d) Bi-Directional-Leader (BDL). Via intra-vehicle communication (e.g., C-V2X according to the meeting report from Federal Communications Commission (POPEO, 2020)), all vehicles share their state information (e.g., the absolute position, the velocity, and the acceleration) with their neighbors according to the IFT. It is assumed that each CAV is equipped with i) an on-board radar responsible for collision detection via measuring the gap distance between any two consecutive vehicles, ii) a built-in GPS sensor for measuring the longitudinal position, iii) a wireless on-board unit for communicating potentially useful information with its proximal vehicles via the C-V2X communication (Verizon North, 2020), iv) an upper-level controller for calculating the desired longitudinal acceleration based on the parameters obtained, and v) a lower-level controller for determining the throttle and brake actuator inputs so as to track the desired acceleration. Such an assumption is reasonable because the sensing, communication, and actuation units required above are available in modern CAVs and therefore do not require specific changes to the existing vehicle configuration. Note that the information of the surrounding obtained by on-board radar only function as the validation data in case of communication unavailability or failure, as more accurate information can be more efficiently obtained through communication.

3.1. Vehicle longitudinal dynamic Modeling

A vehicle longitudinal dynamic model mainly consists of the engine, throttle and brake actuators, drive train, transmission, and torque converter. According to Newton's second law, the longitudinal dynamics of vehicle i considering a variety of resistance forces can be modeled by the following equation:

$$m_i a_i(t) = f_i^e(t) - f_i^g(t) - f_i^w(t) - f_i^r(t), \quad (4)$$

where m_i stands for the unknown mass of vehicle i ; $f_i^e(t)$ is the desired engine force acting on vehicle i ; $f_i^g(t)$, $f_i^w(t)$, and $f_i^r(t)$ denote the gravity component parallel to the road surface, air resistance force, and rolling resistance force, respectively.

The nonlinearity of the system (4) is not conducive to controller design. Therefore, a feedback control input in Appendix A is employed to convert it into a linear form (Wang, 2018):

$$\tau_i \dot{a}_i(t) + a_i(t) = u_i(t), \quad (5)$$

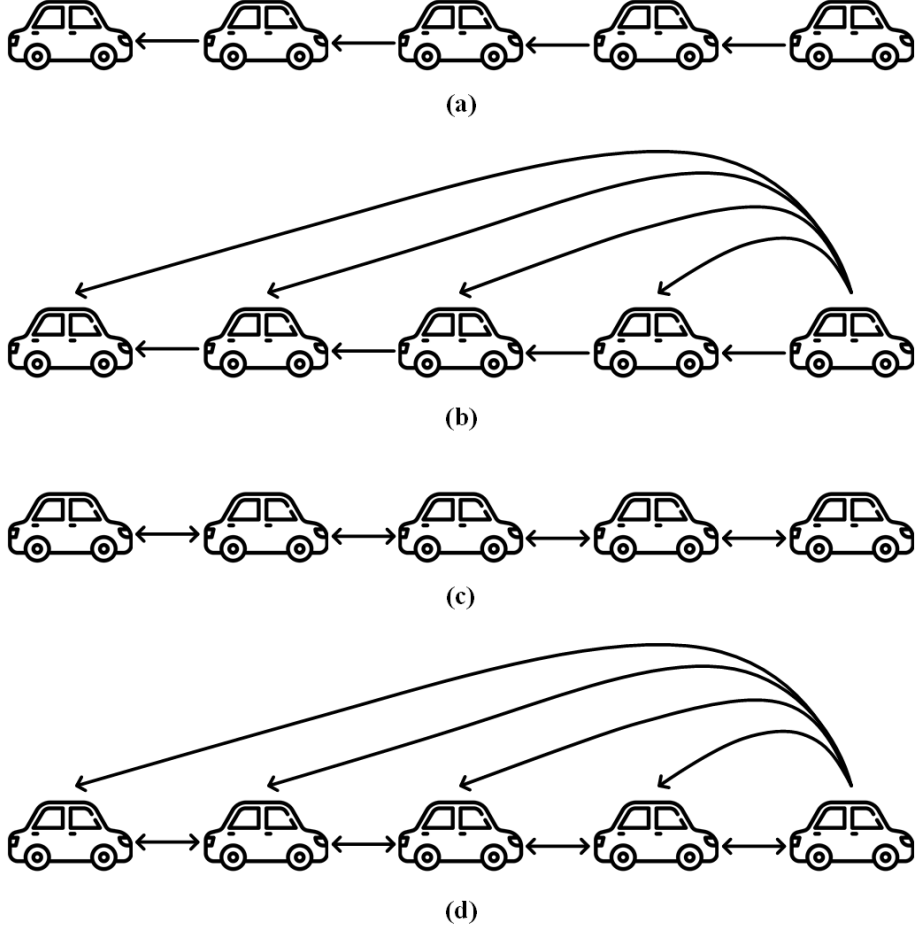


Figure 1: The schematic of the CAV platoon with typical IFTs: (a) Predecessor-Follower (PF); (b) Predecessor-Leader-Follower (PLF); (c) Bi-Directional (BD); and (d) Bi-Directional-Leader (BDL).

where $u_i(t)$ denotes the control input of the lower-level controller, which can be interpreted as the desired acceleration of vehicle i , τ_i is the time constant representing the engine actuator delay.

Reformulate Equation (5), the state space equation can be represented as:

$$\dot{x}_i(t) = Ax_i(t) + Bu_i(t), \quad (6)$$

$$\text{with } A = \begin{bmatrix} 0 & 1 & 0 \\ 0 & 0 & 1 \\ 0 & 0 & -\frac{1}{\tau_i} \end{bmatrix} \text{ and } B = \begin{bmatrix} 0 \\ 0 \\ \frac{1}{\tau_i} \end{bmatrix},$$

where $x_i(t) = [p_i(t) \ v_i(t) \ a_i(t)]^T \in \mathbb{R}^3$ denotes the state vector of vehicle i .

Subject to limited communication, the input for vehicle i are controlled by an appropriate decentralized coupling protocol of communication information:

$$u_i = u_i \underbrace{\left(x_1(t-h(t)), \dots, x_i(t), \dots, x_n(t-h(t)) \right)}_n, \quad (7)$$

where $h(t)$ represents the communication delay within the transmission range which assumed to be time-varying according to the variation of the surrounding environment (Jia and Ngoduy, 2016; Vukadinovic et al., 2018; Vu et al.,

2020; Martín-Sacristán et al., 2020; Pirani et al., 2022). And it satisfies the following constraints:

$$h(t) \in [h_m, h_M], \quad \dot{h}(t) \in [d_m, d_M], \quad \forall t \geq 0, \quad (8)$$

where $0 \leq h_m \leq h_M$ and $d_m \leq d_M \leq 1$.

Here we assume that CAVs adopt the Constant Time Headway (CTH) policy in which CAVs maintain a desired time headway from the reference vehicle. Then the cooperative tracking problem of vehicle i can be formulated as:

$$\begin{cases} \lim_{t \rightarrow \infty} \left\| \sum_{j=1}^n \left| p_i(t) - p_j(t - h(t)) + h_{ij} v_i(t) \right| \right\| = 0, \\ \lim_{t \rightarrow \infty} \left\| \sum_{j=1}^n \left| v_i(t) - v_j(t - h(t)) \right| \right\| = 0, \quad \forall i = 1, \dots, N, \\ \lim_{t \rightarrow \infty} \left\| \sum_{j=1}^n \left| a_i(t) - a_j(t - h(t)) \right| \right\| = 0. \end{cases} \quad (9)$$

where $h_{ij} = -h_{ji}$ stands for the constant time headway between vehicle i and vehicle j .

The consensus goal (9) can be achieved by using an appropriate distributed control strategy. Therefore, the vehicle i adjusts its dynamics through the following decentralized coupling protocol computed onboard as:

$$u_i = - \sum_{j=1}^n a_{ij} k_{ij}^T \begin{bmatrix} p_i(t) - p_j(t - h(t)) + h_{ij} v_i(t) & v_i(t) - v_j(t - h(t)) & a_i(t) - a_j(t - h(t)) \end{bmatrix}^T, \quad (10)$$

where a_{ij} denotes the weight of edge (i, j) and $a_{ij} = 0$ if there is no edge (i, j) ; $k_{ij} = [\alpha_{ij} \quad \beta_{ij} \quad \gamma_{ij}]^T \in \mathbb{R}^{3 \times 1}$ presents the feedback control gain vector, with α_{ij} , β_{ij} , and γ_{ij} denoting the control gain of spacing error, speed error, and acceleration error, respectively.

3.2. CAV platoon Modeling

To prove the consensus of systems (6) and (7) under the action of coupling protocol (10), then the decentralized coupling protocol (10) can be reformulated as:

$$u_i = - \sum_{j=1}^n a_{ij} k_{ij}^T [\psi_{ij} x_i(t) - x_j(t - h(t))], \quad (11)$$

where $\psi_{ij} = \begin{bmatrix} 1 & h_{ij} \\ & 1 \\ & & 1 \end{bmatrix}$ denotes the relationship between the states based on the CTH policy.

Therefore, the dynamics of the error system can be presented as:

$$\begin{cases} \dot{\tilde{p}}_i = \tilde{v}_i, \\ \dot{\tilde{v}}_i = \tilde{a}_i, \\ \dot{\tilde{a}}_i = -\frac{1}{\tau} \tilde{a}_i - \frac{1}{\tau} \sum_{j=1}^n a_{ij} k_{ij}^T (\psi_{ij} x_i(t) - x_j(t - h(t))). \end{cases} \quad (12)$$

From Equation (12), the dynamics of the closed-loop vehicular network can be recast in a compact form with supermatrices as:

$$\dot{x}_i(t) = Ax_i(t) - B \sum_{j=1}^n a_{ij} k_{ij}^T (\psi_{ij} x_i(t) - x_j(t - h(t))). \quad (13)$$

Theorem 3 The CAV platoon under CTH policy with time-varying communication delay can be modeled as a linear time-invariant state time-varying delay system:

$$\begin{cases} \dot{X}(t) = \Psi X(t) + \Psi_d X(t - h(t)), & \forall t \geq 0 \\ X(t) = \phi(t), & \forall t \in [-h, 0] \end{cases} \quad (14)$$

with

$$\left\{ \begin{array}{l} \Psi = A^* - B^* \mathcal{F} E_1 \in \mathbb{R}^{3n \times 3n} \\ \Psi_d = B^* \mathcal{J} E_2 \in \mathbb{R}^{3n \times 3n} \\ A^* = I_n \otimes A \in \mathbb{R}^{3n \times 3n} \\ B^* = I_n \otimes B \in \mathbb{R}^{3n \times n} \\ \mathcal{K} = [k_{ij}^T]_{n \times n} \\ \mathcal{H} = \mathcal{A} \circ \mathcal{K} = [a_{ij} \otimes k_{ij}^T]_{N \times N} \in \mathbb{R}^{n \times 3n} \\ \mathcal{J} = \text{diag} \underbrace{\{D_1, D_2, \dots, D_N\}}_n \in \mathbb{R}^{n \times 3n^2} \\ D_i = \underbrace{[a_{i1} k_{i1}^T, a_{i2} k_{i2}^T, \dots, a_{in} k_{in}^T]}_n \in \mathbb{R}^{1 \times 3n}, \forall i \in \mathcal{V} \\ \mathcal{F} = \text{diag} \underbrace{\{\mathcal{H}_1, \mathcal{H}_2, \dots, \mathcal{H}_N\}}_n \in \mathbb{R}^{n \times 3n^2} \\ \mathcal{H}_i = D_i \circ \underbrace{[\psi_{i1}, \psi_{i2}, \dots, \psi_{in}]}_n \in \mathbb{R}^{1 \times 3n}, \forall i \in \mathcal{V} \\ E_1 = \text{diag} \underbrace{\{I_1, I_1, \dots, I_1\}}_n \in \mathbb{R}^{3n^2 \times 3n} \\ E_2 = \underbrace{[I_2^T \ \dots \ I_2^T]}_n^T \in \mathbb{R}^{3n^2 \times 3n} \\ I_1 = \underbrace{[I_3^T \ \dots \ I_3^T]}_n^T \in \mathbb{R}^{3n \times 3} \\ I_2 = I_{3n} \in \mathbb{R}^{3n \times 3n} \\ I_3 = I_3 \in \mathbb{R}^{3 \times 3} \end{array} \right. \quad (15)$$

where $X(t) = [x_1^T \ \dots \ x_n^T]^T \in \mathbb{R}^{3n}$ stands for the error state vector of the closed-loop vehicular network; ϕ is the initial conditions; Ψ and Ψ_d are constant matrix according to their definitions.

4. Stability analyses

In the context of the stability analysis of state delay systems, the Lyapunov-Krasovskii Stability Theorem is a well-known approach extending the second Lyapunov method dedicated to stability analysis (Gu et al., 2003). It includes the "energy" functionals that are positive definite, and decreasing along the trajectories of the system. The Lyapunov-Krasovskii Theorem is stated below:

Lemma 4 (Lyapunov-Krasovskii Stability Theorem) (Gu and Liu, 2009). Given system (14), suppose that f maps $\mathbb{R} \times (\text{bounded sets in } \mathbb{R}^n \times C)$ into bounded sets in \mathbb{R}^n , and that $u, v, w : \mathbb{R}_+ \rightarrow \mathbb{R}_+$ are continuous nondecreasing functions, where additionally $u(s)$ and $v(s)$ are positive for $s > 0$, and $u(0) = v(0) = 0$. If there exists a functional $V : \mathbb{R} \times \mathbb{R}^n \times C \rightarrow \mathbb{R}$ such that

$$\begin{cases} u(|\phi(0)|) \leq V(t, \phi) \leq v(|\phi|_h), \\ \dot{V}(t, \phi) \leq -w(|\phi(0)|). \end{cases} \quad (16)$$

Then the trivial solution of the system (14) is uniformly stable. If $w(s) > 0$ for $s > 0$, then it is uniformly asymptotically stable. If, in addition, $\lim_{s \rightarrow \infty} u(s) = +\infty$, then it is globally uniformly asymptotically stable. Such a functional V is called a Lyapunov-Krasovskii functional (LKF).

The primary idea of Lemma 4 is to determine a positive definite functional whose derivative with respect to time along the trajectories of the system (14) is negative definite. In the context of the stability analysis of such systems using LKF, several types of functionals have been provided in the literature. Among them, an integral quadratic term is one of the most relevant components of LKF (Pepe and Jiang, 2006):

$$V(X_t) = \int_{-h}^0 \int_{\theta}^0 \dot{X}_t^T(s) R \dot{X}_t(s) ds d\theta, \quad (17)$$

where $\dot{X}_t(s) = \dot{X}(t+s)$ denotes the state of the state delay system, $R > 0$ and $h > 0$.

The positivity of LKF (17) is ensured by $R > 0$. Then another that needs to be clarified is the negation of its derivative. Differentiating this term with respect to the time t , we get:

$$\dot{V}(X_t) = h \dot{X}^T(t) R \dot{X}(t) - \int_{-h}^0 \dot{X}^T(s) R \dot{X}(s) ds. \quad (18)$$

In order to transform Equation (18) into a suitable LMI setup, an over-approximate process of the integral terms is adopted since it cannot be straightforwardly converted in the quadratic formulation described above. Therefore, the next problem is to provide a new lower bound of integral quadratic terms of the form:

$$F(\omega) = \int_{-h}^0 \omega^T(s) R \omega(s) ds, \quad (19)$$

where ω is a continuous function from $[a, b] \rightarrow \mathbb{R}^n$ and consequently integrable.

Corollary 5 Consider a given matrix $R > 0$. Then, for all continuous function ω in $[a, b] \rightarrow \mathbb{R}^n$ the following inequality holds:

$$F(\omega) \geq \frac{1}{h} \left(\int_{-h}^0 \omega(u) du \right)^T R \left(\int_{-h}^0 \omega(u) du \right) + \frac{3}{h} \Omega^T R \Omega, \quad (20)$$

where $\Omega = \int_{-h}^0 \omega(s) ds - \frac{2}{h} \int_{-h}^0 \int_{-h}^s \omega(r) dr ds$.

Proof We first construct the function z for all $u \in [a, b]$ as:

$$z(u) = \int_{-h}^u \omega(s) ds - \frac{u+h}{h} \int_{-h}^0 \omega(s) ds - \frac{(-u)(u+h)}{h^2} \Theta, \quad (21)$$

where Θ is a constant vector of \mathbb{R}^n to be defined. Moreover, the function $z(u)$ (21) satisfies the constraints of Lemma 1, that is $z(0) = z(-h) = 0$ according to its definition.

Then, calculating the left-hand-side of the inequality stated in Lemma 1 leads to:

$$\begin{aligned} \int_{-h}^0 \dot{z}^T(u) R \dot{z}(u) du &= \int_{-h}^0 \omega^T(u) R \omega(u) du - \frac{1}{h} \left(\int_{-h}^0 \omega(u) du \right)^T R \left(\int_{-h}^0 \omega(u) du \right) \\ &\quad + \int_{-h}^0 \left(\frac{(h+2u)}{h^2} \right)^2 du \Theta^T R \Theta - 2 \Theta^T R \int_{-h}^0 \left(\frac{-h-2u}{h^2} \right) \omega(u) du \\ &\quad + 2 \int_{-h}^0 \left(\frac{(-h-2u)}{h^2} \right) du \Theta^T R \left(\int_{-h}^0 \omega(u) du \right). \end{aligned} \quad (22)$$

Substituting $\int_{-h}^0 -h - 2u du = 0$ and applying integration by parts, Equation (22) can be simplified as follows:

$$\begin{aligned} \int_{-h}^0 \dot{z}^T(u) R \dot{z}(u) du &= \int_{-h}^0 \omega^T(u) R \omega(u) du - \frac{1}{h} \left(\int_{-h}^0 \omega(u) du \right)^T R \left(\int_{-h}^0 \omega(u) du \right) \\ &\quad - \frac{3}{(b-a)} \Omega^T R \Omega + \frac{1}{3(b-a)} (\Theta + 3\Omega)^T R (\Theta + 3\Omega). \end{aligned} \quad (23)$$

Substituting $\int_{-h}^0 z(u)du = -\frac{h}{6}(\Theta + 3\Omega)$ and applying Lemma 1, it yields:

$$\begin{aligned} F(\omega) &\geq \frac{1}{h} \left(\int_{-h}^0 \omega(u)du \right)^T R \left(\int_{-h}^0 \omega(u)du \right) + h\Omega^T R\Omega \\ &\quad + \frac{\pi^2 - 12}{36h} (\Theta + 3\Omega)^T R (\Theta + 3\Omega). \end{aligned} \quad (24)$$

Since $\frac{\pi^2 - 12}{36h} > 0$, the third term in the right-hand side of the inequality (24) is definite positive independently of the choice of Θ . Moreover, the inequality is equivalent to equality if and only if $\Theta = -3\Omega$. Furthermore, the definite positiveness of $F(\omega)$ is guaranteed by $R > 0$. This concludes the proof.

Remark 6 Note that the first term to the right of Inequality (20) is Jensen inequality (Gu et al., 2003). Since the second term is definite positive, the lower bound of the integral is clearly higher than the result obtained through Jensen inequality. Therefore, with Wirtinger-Based on Integral Inequality, more accurate stability conditions can be obtained.

According to Inequality (18), another lower bound needed to be determined is the case of $F(\dot{\omega})$. Therefore, Corollary 5 is rewritten as follows:

Corollary 7 For a given matrix $R > 0$, the following inequality holds for all continuously differentiable function ω in $[a, b] \rightarrow \mathbb{R}^n$:

$$F(\dot{\omega}) \geq \frac{1}{h} (\omega(0) - \omega(-h))^T R (\omega(0) - \omega(-h)) + \frac{3}{h} \tilde{\Omega}^T R \tilde{\Omega}, \quad (25)$$

where $\tilde{\Omega} = \omega(0) + \omega(-h) - \frac{2}{h} \int_a^b \omega(u)du$.

Then the following stability theorem is provided.

Theorem 8 Assume that there exist $P \in \mathbb{S}_{3n}^+$, three matrices $S, R, Q \in \mathbb{S}_n^+$, and $X \in \mathbb{S}_{2n}$ such that the following LMIs are satisfied for $h = \{h_m, h_M\}$ and $\dot{h} = \{\dot{d}_m, d_M\}$.

$$\Phi_1(h, \dot{h}) = \Phi_0(h, \dot{h}) - \frac{1}{h_M} \Gamma^T \Phi_2 \Gamma < 0, \quad (26)$$

$$\Phi_2 = \begin{bmatrix} \tilde{R} & X \\ * & \tilde{R} \end{bmatrix} > 0, \quad (27)$$

where

$$\Phi_0(h, \dot{h}) = \text{He}(G_1^T(h)PG_0(\dot{h})) + \hat{S} + \hat{Q}(\dot{h}) + h_M G_0^T(\dot{h})\hat{R}G_0(\dot{h});$$

$$\Gamma = [K_1^T \ K_2^T]^T;$$

$$K_1 = \begin{bmatrix} I & -I & 0 & 0 & 0 \\ I & I & 0 & -2I & 0 \end{bmatrix};$$

$$K_2 = \begin{bmatrix} 0 & I & -I & 0 & 0 \\ 0 & I & I & 0 & -2I \end{bmatrix};$$

$$\hat{Q}(\dot{h}) = \text{diag}(Q, -(1 - \dot{h})Q, 0_{3n});$$

$$\hat{S} = \text{diag}(S, 0, -S, 0_{2n});$$

$$\hat{R} = \text{diag}(R, 0_{3n});$$

$$\tilde{R} = \text{diag}(R, 3R);$$

$$G_0(\dot{h}) = \begin{bmatrix} \Psi & \Psi_d & 0 & 0 & 0 \\ I & -(1 - \dot{h})I & 0 & 0 & 0 \\ 0 & (1 - \dot{h})I & -I & 0 & 0 \\ I & 0 & 0 & 0 & 0 \\ 0 & 0 & 0 & hI & 0 \end{bmatrix};$$

$$G_1(h) = \begin{bmatrix} 0 & 0 & 0 & 0 & 0 \\ 0 & 0 & 0 & hI & 0 \\ 0 & 0 & 0 & 0 & (h_M - h)I \end{bmatrix}.$$

Then the system (14) is asymptotically stable for all delay function h satisfying (8).

Proof We first construct the LKF as:

$$\begin{aligned} V(h, x_t, \dot{x}_t) &= \tilde{x}^T(t)P\tilde{x}(t) + \int_{-h(t)}^0 x^T(s)Qx(s)ds \\ &\quad + \int_{-h_M}^0 x^T(s)Sx(s)ds + \int_{-h_M}^0 \int_{\theta}^0 \dot{x}^T(s)R\dot{x}(s)ds d\theta, \end{aligned} \quad (28)$$

where $\tilde{x}(t) = [x^T(t), \int_{-h(t)}^0 x^T(s)ds, \int_{-h_M}^{-h(t)} x^T(s)ds]^T$.

The positivity of LKF (28) is ensured by $P > 0$, $Q > 0$, $S > 0$, and $R > 0$. Then, the negation of its derivative needs to be clarified. Differentiating the functional (18) along the trajectories of (14) leads to:

$$\dot{V}(h, x_t, \dot{x}_t) = \zeta_1^T(t)\Phi_0(h, \dot{h})\zeta_1(t) - \int_{-h_M}^0 \dot{x}^T(s)R\dot{x}(s)ds, \quad (29)$$

$$\text{where } \zeta_1(t) = \begin{bmatrix} x(t) \\ x(t-h(t)) \\ x(t-h_M) \\ \frac{1}{h(t)} \int_{-h(t)}^0 x(s)ds \\ \frac{1}{h_M-h(t)} \int_{-h_M}^{-h(t)} x(s)ds \end{bmatrix}.$$

Notice the Equation (29) can be obtained by substituting $\tilde{x}(t) = G_1(h)\zeta_1(t)$ and $\dot{\tilde{x}}(t) = G_0(\dot{h})\zeta_1(t)$ into the partial differential of Equation (28).

Then split the integral interval of Equation (29) into two parts: $[-h_M, -h(t)]$ and $[-h_M, 0]$, and apply Corollary 7 respectively to get:

$$-\int_{t-h_M}^t \dot{x}^T(s)R\dot{x}(s)ds \leq -\zeta_1^T(t) \left(\frac{1}{h(t)} K_1^T \tilde{R} K_1 + \frac{1}{h_M - h(t)} K_2^T \tilde{R} K_2 \right) \zeta_1(t). \quad (30)$$

According to the constraint of the Lemma 2, assume there exists a X so that $\Phi_2 > 0$, then the following inequality holds:

$$-\int_{t-h_M}^t \dot{x}^T(s)R\dot{x}(s)ds \leq -\frac{1}{h_M} \zeta_1^T(t) \Gamma^T \Phi_2 \Gamma \zeta_1(t), \quad (31)$$

Substituting Inequality (31) into Equation (29), it yields:

$$\begin{aligned} \dot{V}(h, x_t, \dot{x}_t) &\leq \zeta_1^T(t)\Phi_0(h, \dot{h})\zeta_1(t) - \frac{1}{h_M} \zeta_1^T(t) \Gamma^T \Phi_2 \Gamma \zeta_1(t) \\ &= \zeta_1^T(t) \left(\Phi_0(h, \dot{h}) - \frac{1}{h_M} \Gamma^T \Phi_2 \Gamma \right) \zeta_1(t) \\ &= \zeta_1^T(t)\Phi_1(h, \dot{h})\zeta_1(t). \end{aligned} \quad (32)$$

Equation (32) guarantees $\dot{V}(h, x_t, \dot{x}_t)$ is negative definite by restraining $\Phi_1(h, \dot{h}) < 0$. Since the matrix $\Phi_1(h, \dot{h})$ is affine, and consequently convex, with respect to $h(t)$ and $\dot{h}(t)$, it is necessary and sufficient to ensure that $\Phi_1(h, \dot{h}) < 0$ stays at the vertices of the intervals $[0, h_M] \times [d_m, d_M]$. In summary, $\dot{V}(h, x_t, \dot{x}_t)$ is negative definite if there exists a matrix X such that $\Phi_2 > 0$ and if $\Phi_1(h, \dot{h}) < 0$, for all $(h, \dot{h}) \in [0, h_M] \times [d_m, d_M]$. This concludes the proof.

Remark 9 The primary idea of the Lyapunov-Krasovskii stability theorem is that it is not necessary to ensure the negative definiteness of $V(t, x(t))$ along all the trajectories of the system. Indeed, it is sufficient to ensure its negative definiteness only for the solutions that tend to escape the neighborhood of $V(t, x(t)) \leq c$ of the equilibrium. The specific theoretical analysis is conducted in detail in Appendix B.

Remark 10 The code for constructing the LMIs in Theorem 8 has been uploaded to GitHub for subsequent research. The corresponding URL is attached in Appendix C.

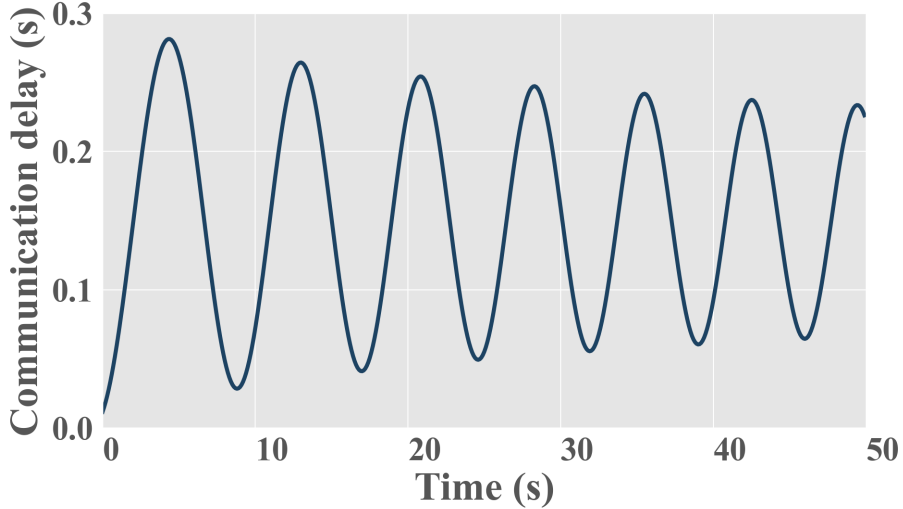


Figure 2: The curve of time-varying communication delay.

5. Numerical analyses

In this section, extensive numerical simulations and analyses on the tracking performance and safety conditions of CAV platoon with different feedback control gains employing the PLF are conducted to illustrate the main results. In addition, the tracking performance of the CAV platoon employing the other three IFTs is also investigated.

5.1. Numerical Setup

To provide a comprehensive performance evaluation analysis, we consider a CAV platoon consisting of 5 CAVs interconnected by the PLF shown in Fig. 1 (b). The Leader CAV drives under a given speed profile while the other CAVs drive under the control strategy. It is worth clarifying that each CAV in the platoon communicates only with the neighbors set in the PLF. Additionally, the control parameters need to be set according to the specific control strategy in practice. For further analysis, parameters for both network and traffic simulation are set in Table 1, for simplicity but without loss of generality. It should be noted that the weights of the weighted adjacency matrix are set to $a_{ij} = \frac{1}{d_i}, \forall (i, j) \in \mathcal{E}$ in order to denote that the information of each neighbor has an equal impact on the control decision. As for the time-varying delay, the time-varying equation is given below in the form of the Bessel function of the first kind, whose time-varying curve is shown in Fig. 2, satisfying the constraint in Equation (8):

$$J_{40}(t) = \sum_{k=0}^{\infty} \frac{(-1)^k}{k!(k+40)!} \left(\frac{t+30}{2} \right)^{2k+40}, \quad t \geq 0. \quad (33)$$

Moreover, for the sake of evaluating the tracking performance under the PLF with different feedback control gains of the CAV platoon, we adopt two representative leader maneuvers, namely:

1. **Trapezoidal signal:** The leader suddenly decelerates to $14.6m/s$ at $-0.15m/s^2$ and keeps it for $36s$. Then the leader accelerates back to $20m/s$ at $0.3m/s^2$ (see Fig. 3(a, b)).
2. **Oscillation signal:** The leader suddenly accelerates to $23.6m/s$ in $12s$ and keeps the velocity for $15s$. Then the leader decelerates to $16.4m/s$ in $12s$ and accelerates back to $20m/s$ in $12s$ (see Fig. 3(c, d)).

5.2. Numerical analyses of the CAV platoon under the PLF

In this subsection, the CAV platoon employing the PLF is taken as the object of analysis, where each CAV in the platoon takes the same control parameters that meet the Theorem 8. In addition, in order to investigate the effect of different feedback control gains on tracking performance, the following four feedback control gains are selected:

1. *Parameter I:* $k_i = [0.3, 0.3, 0.3]^T$;

Table 1
Network and traffic simulation parameters.

Parameters	Value
Platoon size n	5 vehicles
Vehicle length L	5 [m]
Engine actuator delay τ_i	0.2 [s] ¹
Weight of edge (i, j) a_{ij}	$\frac{1}{d_i}$
Minimum communication delay h_m	0 [m]
Maximum communication delay h_M	0.3 [m]
Minimum communication delay slope d_m	-0.1
Maximum communication delay slope d_M	0.1

¹ (Wang et al., 2018; Zhou et al., 2020)

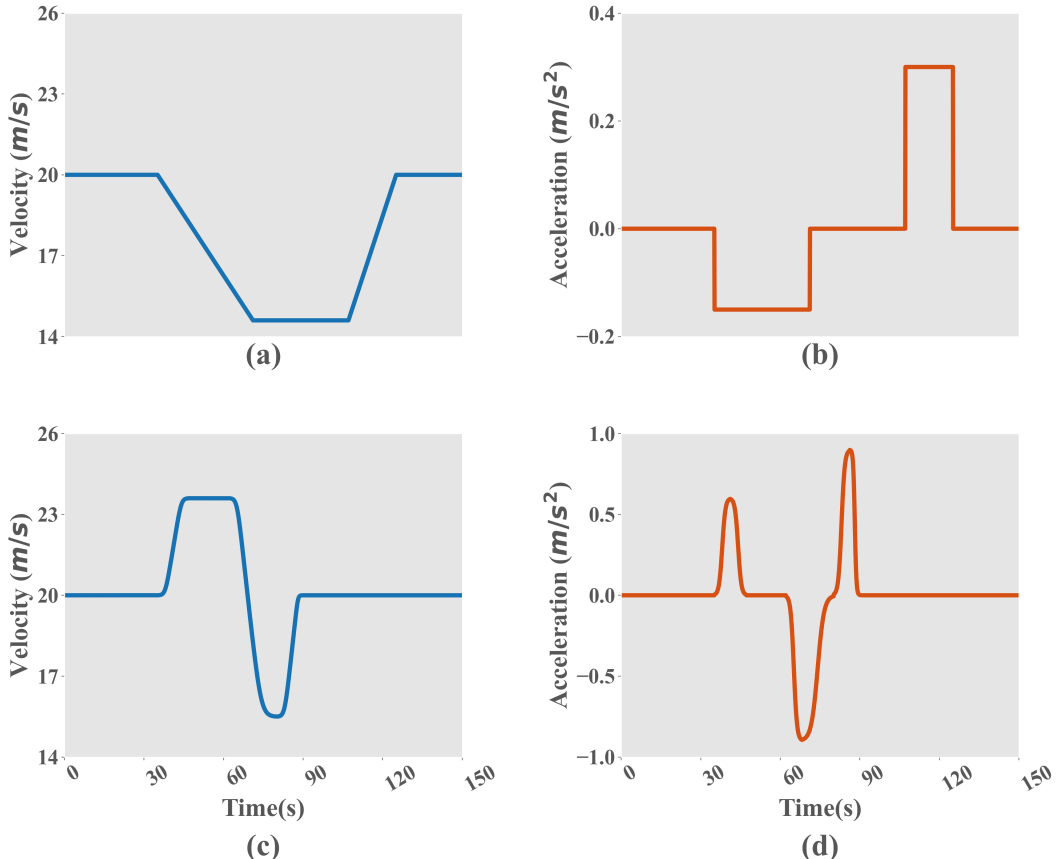


Figure 3: The two representative leader maneuvers: (a) and (b) denotes the velocity and acceleration of the trapezoidal signal, respectively; (c) and (d) denote the velocity and acceleration of the oscillation signal, respectively.

2. *Parameter II:* $k_i = [1, 0.3, 0.3]^T$;
3. *Parameter III:* $k_i = [0.3, 1, 0.3]^T$;
4. *Parameter IV:* $k_i = [0.3, 0.3, 1]^T$.

Moreover, the desired time headway is set to $h_i = 0.6s$. Corresponding matrixes P, S, Q, R , and X can be found in Appendix C. Moreover, a detailed analysis is carried out on the tracking performance and safety conditions.

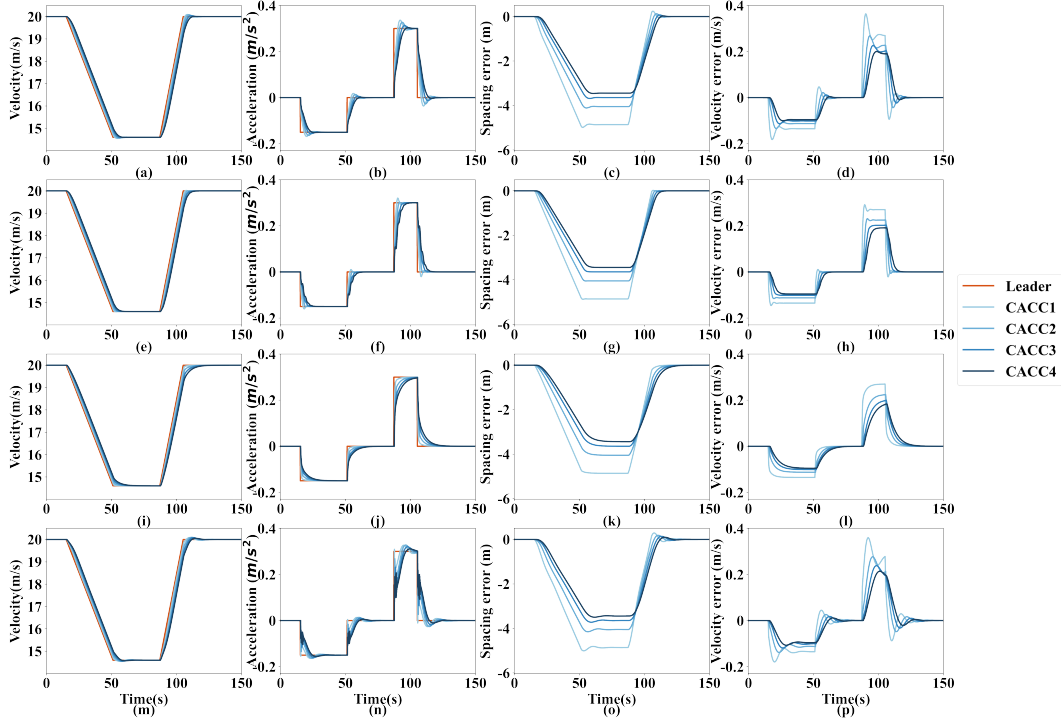


Figure 4: Tracking performance of the CAV platoon for the Trapezoidal signal in Fig. 3(a,b) under the four feedback control gains: (a), (b), (c), and (d) present tracking results under Parameter I, including the velocity, tracking error of spacing, tracking error of velocity, and tracking error of acceleration, respectively; (e), (f), (g), and (h) show the case under Parameter II; (i), (j), (k), and (l) denote the case under Parameter III; (m), (n), (o), and (p) show the case under Parameter IV.

5.2.1. Tracking performance analyses

After the CAV platoon is formed and each CAV reaches the equilibrium state where the tracking error is zero, we apply the trapezoidal signal shown in Fig. 3(a,b) as the leader maneuver to evaluate the tracking performance of the four feedback control gains under investigation. The corresponding results are presented in Fig. 4, which shows how the different CAVs in the CAV platoon track the leader motion under the trapezoidal signal.

As expected in the theoretical results, all CAVs are capable of tracking the leader motion smoothly with a steady-state error of 0. Transient variations in leader motion can cause abrupt changes in tracking error, which disappear over time thanks to stability. Another conclusion can be drawn by comparing the cases of different control gains. Although the four control gains are stable, the effect of different gains on the tracking performance differs. By increasing the gain of the spacing and velocity errors, the overshoot of the acceleration curve is significantly reduced, especially in the case of the gain of velocity error, the overshoot is suppressed. However, the increase in the gain of the spacing leads to fluctuations in the acceleration curve, probably due to time-varying delay. For the case of increasing the gain of acceleration error, the tracking performance is undesirable due to the drastic fluctuations, although the stability can also be maintained. Therefore, in terms of control parameter selection, increasing the gain of velocity error within a suitable range can improve the tracking performance to a certain extent.

Furthermore, the tracking performance of the four feedback control gains has also been adopted for the oscillation signal defined in Fig. 3(c, d). The corresponding tracking performance of the four feedback control gains is illustrated in Fig. 5. Under the oscillation signal, the cases under four feedback control gains still maintain excellent tracking performance as shown in Fig. 5, where each vehicle adjusts to changes in leader motion and returns to the equilibrium state with zero steady-state error. Besides, a similar phenomenon and conclusion as in Fig. 4 can be obtained that increasing the gain of spacing and velocity errors can benefit tracking performance while increasing the gain of acceleration errors does not necessarily.

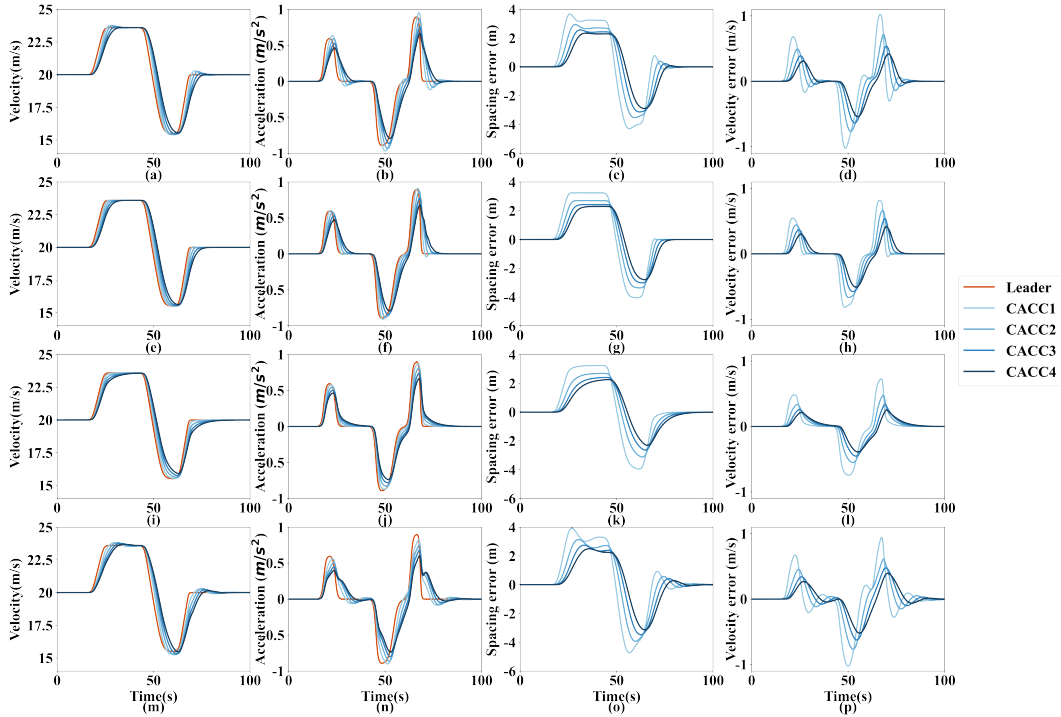


Figure 5: Tracking performance of the CAV platoon for the Oscillation signal in Fig. 3(c,d) under the four feedback control gains: (a), (b), (c), and (d) present tracking results under Parameter I, including the velocity, tracking error of spacing, tracking error of velocity, and tracking error of acceleration, respectively; (e), (f), (g), and (h) show the case under Parameter II; (i), (j), (k), and (l) denote the case under Parameter III; (m), (n), (o), and (p) show the case under Parameter IV.

Moreover, parallel to the stability studied by tracking performance, we selected two widely accepted indicators for evaluating transient response: Setting time (ST) and Number of oscillations (NOO) for further investigation of the transient response performance of different feedback control gains. ST refers to "the time required for the response curve to reach and stay within a range of a certain percentage (2%) of the final value". While NOO refers to "the number of deviations of the response curve from the final value caused by errors in the setting time". Of these two indicators, ST describes the time for the controller to recover from transient response to equilibrium, that is, the speed in the fundamental objective, while NOO is concerned with another fundamental objective, accuracy. Moreover, a smaller NOO means less acceleration and deceleration changes, representing a more comfortable driving experience. Also, since the investigation is on the differences in the transient response of different feedback control gains, the form of the leader motion has little effect on this, so the results are analyzed here only for the case under Trapezoidal signal.

Fig. 6 compares different feedback control gains on the two indicators of transient response. One conclusion that can be obtained is that different control gains indeed affect transient response. Comparing the case of different control gains, the cases of Parameter II and Parameter III have a smaller ST and NOO than the case of Parameter I, which indicates that improving the gain of spacing and velocity errors is indeed effective in reducing the velocity fluctuations and time from the perturbation to the equilibrium state, thus improving driving comfort and safety. However, the results of the Parameter IV show that increasing the gain of acceleration error is not a good idea to improve the transient response. Furthermore, for all cases of control gain, the ST increases and NOO decreases as the vehicle index increases. This illustrates that as the size of the CAV platoon increases, the velocity fluctuation of the CAV from the perturbation to the equilibrium state will be less, although the recovery time will become longer. It is worth mentioning that for the case of Parameter III, the NOO is 0 means that the transient response under this case is not overshoot, which is a great benefit on safety and comfort.

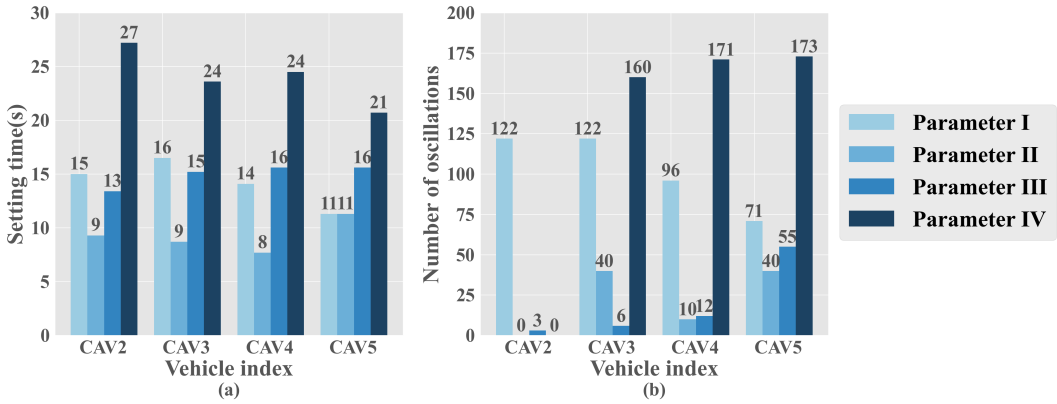


Figure 6: Indicators for evaluating the transient response of each CAV among the CAV platoon under the four feedback control gains: (a) the case of setting time; (b) the case of the number of oscillations.

5.2.2. Safety analyses considering hard braking maneuver

To further evaluate the safety in all the different driving scenarios and feedback control gains, we have also quantitatively analyzed the possible emergence of critical driving situations for all feedback control gains under investigation by exploiting the safety indicator Deceleration Rate to Avoid the Crash (DRAC), which is well known in the literature (Fu and Sayed, 2021a,b). This indicator presents the deceleration rate needed to be applied by a vehicle to avoid a collision with another vehicle which can be defined for each vehicle i at the time t as follows:

$$DRAC_i(t) = \frac{(v_i(t) - v_{i-1}(t))^2}{2(p_{i-1}(t) - p_i(t) - L)}. \quad (34)$$

Moreover, we consider the hard braking maneuver as an additional scenario for evaluation, where the Leader decelerates from $20m/s$ to $0m/s$ within 20s. Fig. 7 displays how the CAV platoon reacts to the hard braking scenario for the four feedback control gains under investigation. Similarly, CAVs in the CAV platoon track the Leader motion accurately and decelerate to $0m/s$ without collision under each control gain. Furthermore, the DRAC of different CAVs under different control gains in the hard braking maneuver is presented as box plots in Fig. 8. It is worth mentioning that the DRAC of the Leader is omitted since it has no predecessor, which will raise the risk of collisions. Besides, the CAV2, CAV3, CAV4, and CAV5 refer to the second, third, fourth, and fifth CAV in the CAV platoon, respectively.

A phenomenon can be observed from Fig. 8 by comparing the boxes that the median DRAC of all CAVs under the Parameter II and Parameter III is significantly lower than that under Parameter I and Parameter V, which is similar to the rough results obtained in the tracking performance analyses. Therefore, we can conclude that increasing the gain of spacing and velocity errors can maintain better safety relative to the gain of acceleration error. Besides, another conclusion can be obtained by comparing different CAVs under the same feedback control gain. That is, although the control parameters are the same, the index in the platoon affects the safety conditions.

5.3. Numerical analyses of the alternative IFTs

In this subsection, the parameters in Table 1 are still adopted for both network and traffic simulation. Moreover, the control parameters are set to $k_i = [0.3, 0.3, 0.3]^T$ and $h_i = 0.6s$. The difference is that the section mainly analyzes the tracking performance of the CAV platoon employed by PF, BD or BDL. It is worth mentioning that the control parameters chosen here still exist matrixes P, S, Q, R , and X satisfy the Theorem 8, which can be found in Appendix C.

As in Section 5.2.1, the Trapezoidal signal defined in Section 5.1 is employed to investigate the tracking performance of different IFTs. The tracking performance of the CAV platoon is presented in Fig. 9.

Good tracking performances have also been verified for alternative IFTs. A similar phenomenon can be observed that the transient response from tracking Leader motion decreases gradually, thanks to stability. It is worth noting that for the case of BD and BDL, the tracking process is smooth; on the contrary, there are significant fluctuations in the tracking process for the case of PF, as disclosed in the recent technical literature (Zheng et al., 2015b).

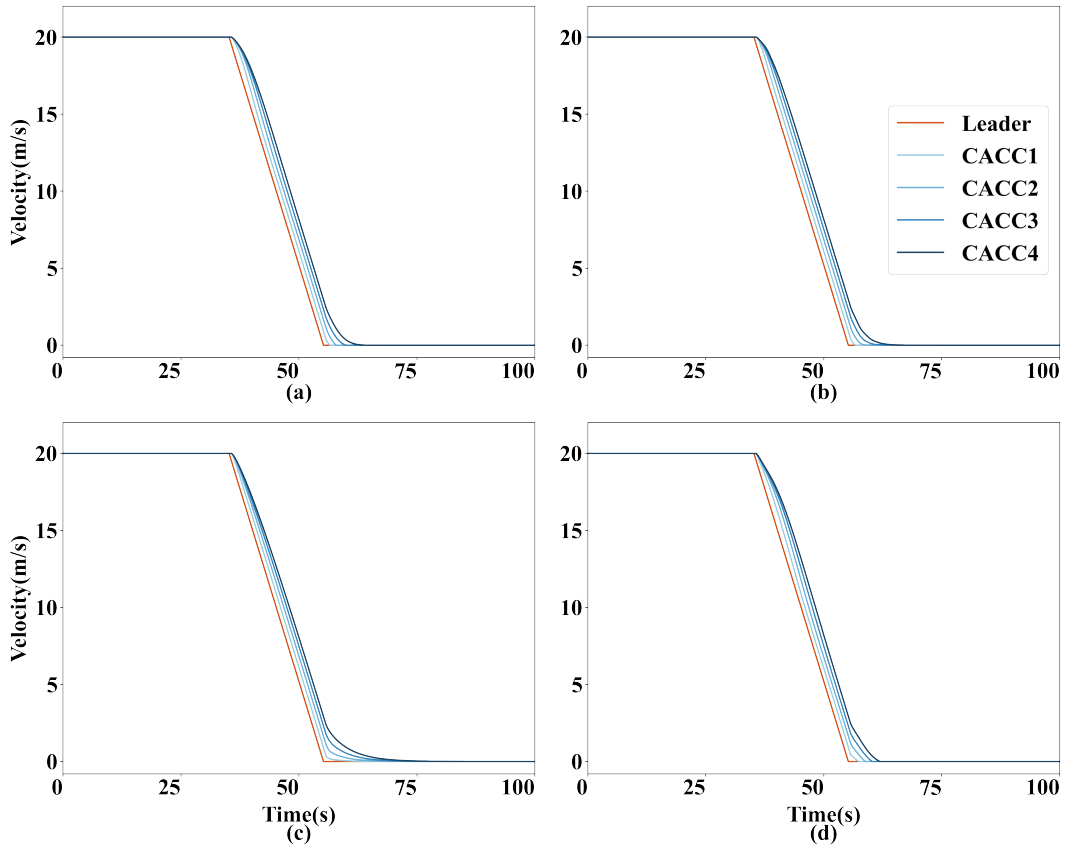


Figure 7: Tracking performance for a hard braking maneuver for each feedback control gain under investigation: (a) Parameter I; (b) Parameter II; (c) Parameter III; (d) Parameter IV.

Similarly, ST and NOO are analyzed to investigate the specific effects of different IFTs on the transient response, and the results are demonstrated in Fig. 10. It can be found that the case under BD has a significantly higher ST than the cases under the other three IFTs. Moreover, although the ST of the cases under all IFTs increases with the increase of the vehicle index, only the case under PF increases significantly while the cases under the other IFTs increase very slightly. One conclusion can be drawn that the CAV platoon with PLF and BDL recovers from the perturbation to the equilibrium state more quickly than PF and BD. In fact, this is caused by direct communication with the leader, thus avoiding hard oscillations during transients.

On the other hand, as the vehicle index increases, for the cases under PLF, BD, and BDL, the NOO decreases, while for the cases under PF, the NOO increases. Furthermore, of the other three IFTs, the case under BD has the largest NOO, and the case under BDL has the smallest. In general, the transient performance can be significantly enhanced by communicating with the leader and bi-directional communication.

6. Conclusion and future work

In this paper, a generic supermatrix modeling approach for the CAV platoon considering time-varying communication delay is proposed. This generic modeling approach consists of applying graph theory to describe the communication relationships within a CAV platoon generally defined by IFT and modeling the linear time-invariant state time-varying delay system corresponding to the CAV platoon that employs a CTH control strategy with the help of supermatrices. Furthermore, based on the properties of the linear time-invariant state time-varying delay system, a novel stability condition of the generic CAV platoon is derived by applying Wirtinger-Based Integral Inequality and Lyapunov-Krasovskii Stability Theorem. Furthermore, extensive numerical analyses are conducted to comprehensively evaluate the tracking performance and safety conditions of four control parameters and thus provide

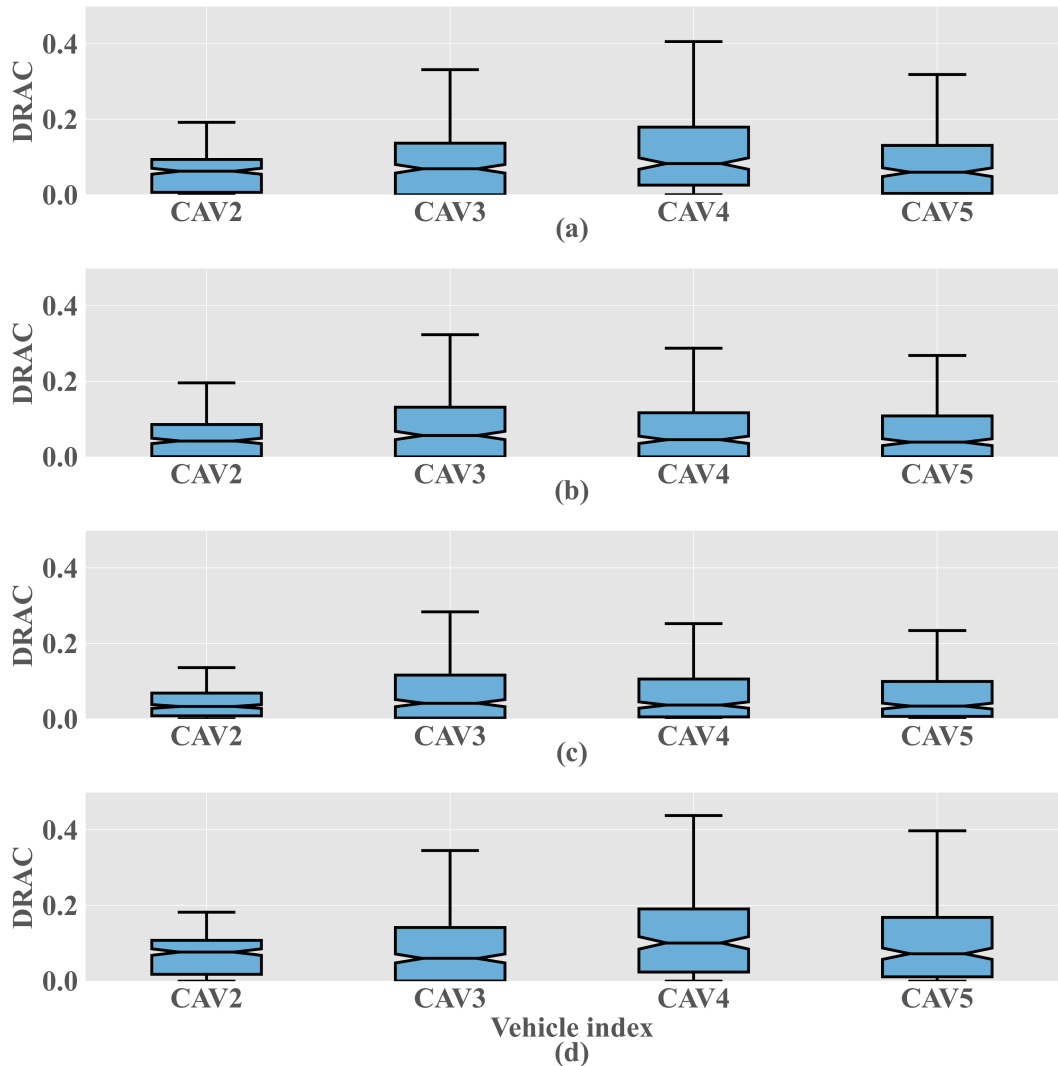


Figure 8: The DRAC boxplots for each CAV of each feedback control gain under investigation: (a) Parameter I; (b) Parameter II; (c) Parameter III; (d) Parameter IV.

guidance for the selection of control parameters. At last, a comparison of the tracking performance between the CAV platoon employing different IFTs sheds some light on the selection of IFTs.

The following conclusions can be drawn through numerical analysis:

1. With the help of the Lyapunov-Krasovskii stability theorem and Wirtinger-Based Integral Inequality, a stability condition considering the time-varying delay for the CAV platoon can be obtained.
2. The CAV platoon adopting the control parameters and IFTs under investigation can achieve smooth tracking of the leader's motion and maintain a safe condition in various scenarios, with stability guaranteed.
3. From the perspective of control parameters, increasing the gain of spacing and velocity errors can benefit tracking performance and safety conditions, while increasing the gain of acceleration errors does not.
4. Taking the IFT perspective, the tracking and transient performance can be significantly enhanced by communicating with the leader and bi-directional communication.

However, we acknowledge that the vehicle behavior in the simulation is only a simplification of reality, and further field experiments are needed for providing a more accurate analysis of the tracking performance. Likewise, the time-varying delay function applied in this paper is an assumed Bessel function satisfying the condition that both the delay

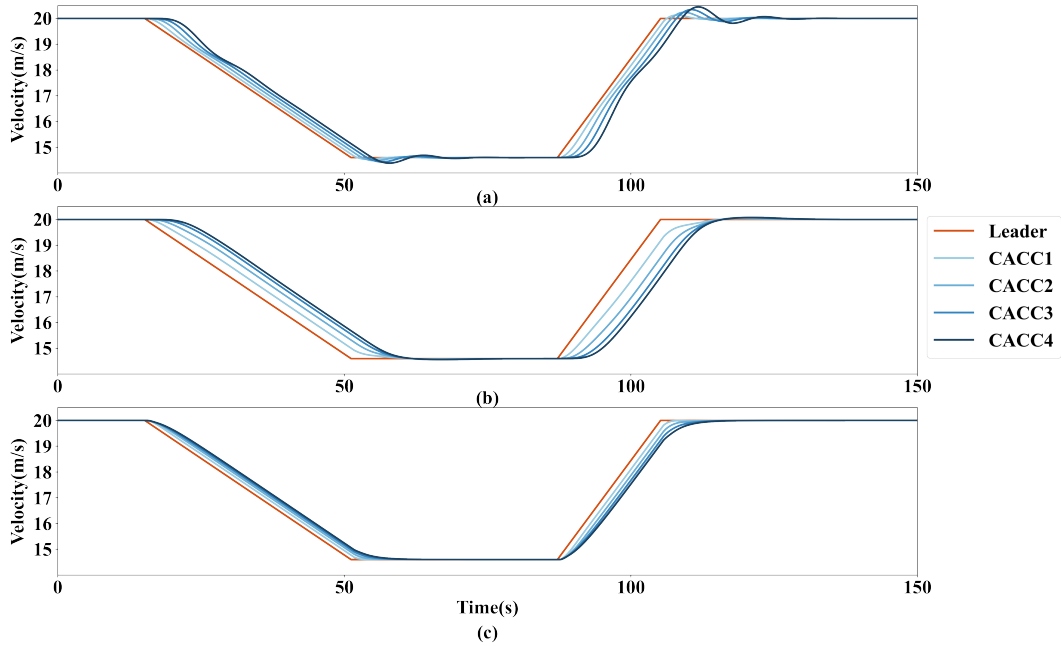


Figure 9: Tracking performance of the CAV platoon for the Trapezoidal signal in Fig. 3(a,b) under the alternative three IFTs: (a) presents tracking results under PF; (b) presents tracking results under BD; (c) denotes the case under BDL.

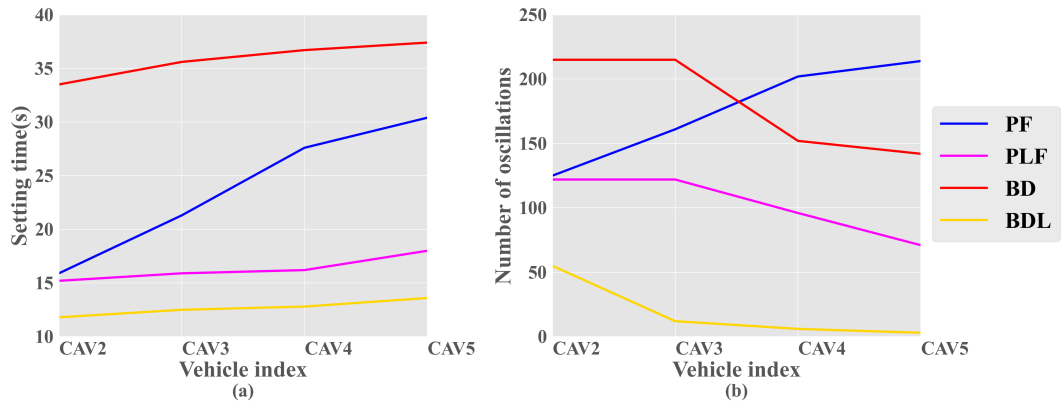


Figure 10: Indicators for evaluating the transient response of each CAV among the CAV platoon under the four IFTs: (a) the case of setting time; (b) the case of the number of oscillations.

and its derivative are bounded, which does not fit the actual time-varying delay perfectly. Therefore, corresponding field experiments should also be conducted to provide insights into the time-varying relationship of communication delays. Furthermore, the control parameter scheme that yields the optimal tracking performance should be further investigated through theoretical research and field experiments. Future research should also be directed toward designing novel control strategies to enable smoother and safer tracking performance.

Appendix A. Feedback control for linearization

In this appendix, we provide the linearization of the longitudinal vehicle dynamic in Equation (4). The functions of the lumped uncertain resistance forces, including $f_i^g(t)$, $f_i^w(t)$, and $f_i^r(t)$ are expressed as follows:

$$\begin{cases} f_i^g(t) = m_i g \sin(\theta_i(t)), \\ f_i^w(t) = \frac{1}{2} \rho C_D A_F (v_i(t) + v_w(t))^2, \\ f_i^r(t) = \mu_R m_i g \cos(\theta_i(t)). \end{cases} \quad (35)$$

where $g = 9.81 \text{m/s}^2$ denotes the acceleration of gravity; $\theta_i(t)$ is the inclination angle of the road; ρ denotes the air density; C_D is the aerodynamic drag coefficient; A_F represents the maximal cross-sectional/frontal area of the vehicle; $v_w(t)$ denotes the uncertain headwind speed; μ_R is the coefficient of rolling resistance.

The desired engine dynamic is modeled as follows:

$$(\tau_i s + 1) F_i^e = U_i. \quad (36)$$

Adopting the inverse Laplace transformation on Equation (36) arrives at:

$$\dot{f}_i^e(t) = \frac{u_i(t)}{\tau_i} - \frac{f_i^e(t)}{\tau_i}. \quad (37)$$

Substituting Equation (4) into Equation (37) and differentiating both sides of Equation (37) with respect to time, we get:

$$\begin{aligned} \dot{a}_l(t) &= \frac{\dot{f}_l^e(t)}{m_i} - \frac{\dot{f}_l^g(t)}{m_i} - \frac{\dot{f}_l^{i\omega}(t)}{m_i} - \frac{\dot{f}_l^r(t)}{m_i} \\ &= \frac{u_i(t)}{m_i \tau_i} \\ &\quad - \frac{a_i(t) + g \sin(\theta_i(t)) [1 - \tau_i \mu_R \dot{\theta}_l(t)] + g \cos(\theta_i(t)) [1 + \tau_i \dot{\theta}_l(t)]}{\tau_i} \\ &\quad - \frac{\frac{1}{2} \rho C_D A_F (v_i(t) + v_w(t)) ((v_i(t) + v_w(t)) + 2\tau_i (a_i(t) + \dot{v}_w(t)))}{\tau_i}. \end{aligned} \quad (38)$$

Thus, the nonlinear state feedback chosen for linearizing can be defined by:

$$\begin{aligned} u_i^*(t) &= m_i u_i(t) + g \sin(\theta_i(t)) [1 - \tau_i \mu_R \dot{\theta}_i(t)] + g \cos(\theta_i(t)) [1 + \tau_i \dot{\theta}_i(t)] \\ &\quad + \frac{1}{2} \rho C_D A_F (v_i(t) + v_w(t)) ((v_i(t) + v_w(t)) + 2\tau_i (a_i(t) + \dot{v}_w(t))). \end{aligned} \quad (39)$$

Under the new feedback control input, the Equation (4) can be rewritten as:

$$\tau_i \dot{a}_i(t) + a_i(t) = u_i(t). \quad (40)$$

Appendix B. Connection between Lyapunov-Krasovskii stability theorem and second Lyapunov method.

First we present a lemma on the Lyapunov function:

Lemma 11 (*Kolmanovskii and Myshkis, 1999*). Let a system $\dot{x}(t) = f(x(t), x(t-h(t)))$ with $f(0,0) = 0$. Assume the Lyapunov function $F : G \rightarrow \mathbb{R}$ exists with $x, y \in G$, $F(y) < F(x)$ implies

$$(F'(x) f(x, y)) (\ddot{F}(x) f(x, y)) \leq 0. \quad (41)$$

Then the solution $x(t) \equiv 0$ is stable.

Suppose there exists a Lyapunov function $F : \mathbb{R}^n \rightarrow \mathbb{R}$. Then define functional $V : C \rightarrow \mathbb{R}$ as follows:

$$V(\phi) := \max_{-h \leq \theta \leq 0} F(\phi(\theta)), (\forall \phi \in C). \quad (42)$$

By definition, the following conditions hold:

$$\dot{V}(\phi) \begin{cases} \leq 0, & \text{if } F(\phi(0)) < V(\phi), \\ = \max (\dot{F}(\phi(0)), f(\phi(0), \phi(-h(t))), 0), & \text{if } F(\phi(0)) = V(\phi), \end{cases} \quad (43)$$

where $f(\phi(0), \phi(-h(t))) = \Psi\phi(0) + \Psi_d\phi(-h(t))$.

Thus $\dot{V}(\phi) > 0$ holds if and only if the following condition holds:

$$F(\phi(0)) = \max_{-h \leq \theta \leq 0} F(\phi(\theta)) \text{ and } (\dot{F}(\phi(0)), f(\phi(0), \phi(-h(t)))) > 0. \quad (44)$$

The function F can be defined in some neighborhood $G \subset \mathbb{R}^n$. And the functional V is then defined for $\phi \in C$ with values in G .

Suppose Equation (44) holds for some functions $\phi \in C$, then we can obtain the inequality $F(\phi(-h(t))) < F(\phi(0))$ making ϕ arbitrarily small. Thus the second condition in Equation (44) still holds, but conflicts with Lemma 11. Therefore $\dot{V}(\phi) \leq 0$ holds constantly for all ϕ .

Hence, the Lyapunov-Krasovskii stability theorem can be regarded as a special case of extending the second Lyapunov method to functional space. However, this special case does not affect the stability results by constraining the definite sign at the start and end points instead of the definite sign in the neighborhood, and thus does not lead to additional constraints in the extension to the functional space. Therefore, the stability conditions obtained based on the Lyapunov-Krasovskii stability theorem are more accurate than those obtained based on the second Lyapunov method. Similar conclusions can be found in much research (Wang et al., 2016; Lian et al., 2020).

Appendix C. Attachments uploaded to GitHub

The uploaded code of this paper contains the model formulation of Theorem 3 and the construction of LMIs for Theorem 8. In addition, the matrices corresponding to the four sets of control parameters for PLF selected in Section 5.2 and three sets for PF, BD, and BDL selected in Section 5.3, which are compatible with Theorem 8, have also been uploaded. The URL of the uploaded file repository is: <https://github.com/ruantiancheng/code-of-paperGeneral-heterogeneous-CAV-platoon-considering-the-time-varying-communication-delay>.

CRediT authorship contribution statement

Tiancheng Ruan: Conceptualization of this study, Methodology, Writing - Original draft preparation, Resources, Software. **Hao Wang:** Formal analysis, Funding acquisition, Supervision, Writing - review & editing. **Zewen Zuo:** Data curation, Investigation. **Gengyue han:** Writing - Original draft preparation. **Beier Ba:** Formal analysis, Writing - Original draft preparation. **Changyin Dong:** Formal analysis, Funding acquisition.

Acknowledgment

This research was sponsored by the National Science Foundation of China (No. 51878161 and No.52072067), Postgraduate Research & Practice Innovation Program of Jiangsu Province (KYCX22_0266), Natural Science Foundation of Jiangsu Province (No. BK20210249) and Jiangsu Planned Projects for Postdoctoral Research Funds (No. SBK2021041144).

References

- van Arem, B., Abbas, M.M., Li, X., Head, L., Zhou, X., Chen, D., Bertini, R., Mattingly, S.P., Wang, H., Orosz, G., 2016. Integrated traffic flow models and analysis for automated vehicles, in: Road Vehicle Automation 3. Springer, pp. 249–258.
 Chang, X., Li, H., Rong, J., Zhao, X., 2020. Analysis on traffic stability and capacity for mixed traffic flow with platoons of intelligent connected vehicles. *Physica A: Statistical Mechanics and its Applications* 557, 124829.

- Dey, K.C., Yan, L., Wang, X., Wang, Y., Shen, H., Chowdhury, M., Yu, L., Qiu, C., Soundararaj, V., 2015. A review of communication, driver characteristics, and controls aspects of cooperative adaptive cruise control (CACC). *IEEE Transactions on Intelligent Transportation Systems* 17, 491–509.
- Fridman, E., 2006. Descriptor discretized lyapunov functional method: analysis and design. *IEEE Transactions on Automatic control* 51, 890–897.
- Fu, C., Sayed, T., 2021a. Comparison of threshold determination methods for the deceleration rate to avoid a crash (drac)-based crash estimation. *Accident Analysis & Prevention* 153, 106051.
- Fu, C., Sayed, T., 2021b. Random parameters bayesian hierarchical modeling of traffic conflict extremes for crash estimation. *Accident Analysis & Prevention* 157, 106159.
- Ghiasi, A., Hussain, O., Qian, Z.S., Li, X., 2017. A mixed traffic capacity analysis and lane management model for connected automated vehicles: A Markov chain method. *Transportation Research Part B: Methodological* 106, 266–292.
- Goñi-Ros, B., Schakel, W.J., Papacharalampous, A.E., Wang, M., Knoop, V.L., Sakata, I., van Arem, B., Hoogendoorn, S.P., 2019. Using advanced adaptive cruise control systems to reduce congestion at sags: An evaluation based on microscopic traffic simulation. *Transportation Research Part C: Emerging Technologies* 102, 411–426. Publisher: Elsevier.
- Gu, K., Chen, J., Kharitonov, V.L., 2003. Stability of time-delay systems. Springer Science & Business Media.
- Gu, K., Liu, Y., 2009. Lyapunov–Krasovskii functional for uniform stability of coupled differential-functional equations. *Automatica* 45, 798–804.
- Herman, R., Montroll, E.W., Potts, R.B., Rothery, R.W., 1959. Traffic dynamics: analysis of stability in car following. *Operations research* 7, 86–106.
- Jia, D., Ngoduy, D., 2016. Enhanced cooperative car-following traffic model with the combination of V2V and V2I communication. *Transportation Research Part B: Methodological* 90, 172–191. Publisher: Elsevier.
- Jin, I.G., Orosz, G., 2016. Optimal control of connected vehicle systems with communication delay and driver reaction time. *IEEE Transactions on Intelligent Transportation Systems* 18, 2056–2070.
- Kamath, G.K., Jagannathan, K., Raina, G., 2015. Car-following models with delayed feedback: local stability and hopf bifurcation, in: 2015 53rd Annual Allerton Conference on Communication, Control, and Computing (Allerton), IEEE. pp. 538–545.
- Kesting, A., Treiber, M., Helbing, D., 2010. Enhanced intelligent driver model to access the impact of driving strategies on traffic capacity. *Philosophical Transactions of the Royal Society A: Mathematical, Physical and Engineering Sciences* 368, 4585–4605. Publisher: The Royal Society Publishing.
- Kolmanovskii, V., Myshkis, A., 1999. Introduction to the Theory and Applications of Functional Differential Equations. Springer Netherlands, Dordrecht. doi:10.1007/978-94-017-1965-0.
- Lhachemi, H., Prieur, C., 2020. Feedback stabilization of a class of diagonal infinite-dimensional systems with delay boundary control. *IEEE Transactions on Automatic Control* 66, 105–120.
- Li, D., Liu, Q., Ju, X., 2021. Uniform decay estimates for solutions of a class of retarded integral inequalities. *Journal of Differential Equations* 271, 1–38. Publisher: Elsevier.
- Li, Y., Chen, Z., Yin, Y., Peeta, S., 2020. Deployment of roadside units to overcome connectivity gap in transportation networks with mixed traffic. *Transportation Research Part C: Emerging Technologies* 111, 496–512. Publisher: Elsevier.
- Li, Y., Sun, D., Cui, M., 2010. Lyapunov stability analysis for the full velocity difference car-following model. *Control Theory & Applications* 12, 014.
- Li, Y., Zhu, H., Cen, M., Li, Y., Li, R., Sun, D., 2013. On the stability analysis of microscopic traffic car-following model: a case study. *Nonlinear Dynamics* 74, 335–343.
- Lian, H.H., Xiao, S.P., Yan, H., Yang, F., Zeng, H.B., 2020. Dissipativity analysis for neural networks with time-varying delays via a delay-product-type lyapunov functional approach. *IEEE transactions on neural networks and learning systems* 32, 975–984.
- Liu, H., Kan, X., Shladover, S.E., Lu, X.Y., Ferlis, R.E., 2018. Impact of cooperative adaptive cruise control on multilane freeway merge capacity. *Journal of Intelligent Transportation Systems* 22, 263–275.
- Martín-Sacristán, D., Roger, S., Garcia-Roger, D., Monserrat, J.F., Spapis, P., Zhou, C., Kaloxyllos, A., 2020. Low-Latency Infrastructure-Based Cellular V2V Communications for Multi-Operator Environments With Regional Split. *IEEE Transactions on Intelligent Transportation Systems* 22, 1052–1067.
- Martyniuk, A.A., Gutovski, R., 1979. Integral inequalities and stability of motion. Kiev Izdatel Naukova Dumka .
- Montanino, M., Punzo, V., 2021. On string stability of a mixed and heterogeneous traffic flow: A unifying modelling framework. *Transportation Research Part B: Methodological* 144, 133–154.
- Navas, F., Milanés, V., 2019. Mixing V2V- and non-V2V-equipped vehicles in car following. *Transportation Research Part C: Emerging Technologies* 108, 167–181. URL: <https://doi.org/10.1016/j.trc.2019.08.021>. doi:10.1016/j.trc.2019.08.021.
- Nikolos, I.K., Delis, A.I., Papageorgiou, M., 2015. Macroscopic Modelling and Simulation of ACC and CACC Traffic, in: IEEE Conference on Intelligent Transportation Systems, Proceedings, ITSC, IEEE. pp. 2129–2134. doi:10.1109/ITSC.2015.344.
- Park, M., Kwon, O., Park, J.H., Lee, S., Cha, E., 2015. Stability of time-delay systems via Wirtinger-based double integral inequality. *Automatica* 55, 204–208. Publisher: Elsevier.
- Park, P., Ko, J.W., Jeong, C., 2011. Reciprocally convex approach to stability of systems with time-varying delays. *Automatica* 47, 235–238. Publisher: Elsevier.
- Pepe, P., Jiang, Z.P., 2006. A Lyapunov–Krasovskii methodology for ISS and iISS of time-delay systems. *Systems & Control Letters* 55, 1006–1014. Publisher: Elsevier.
- Pirani, M., Baldi, S., Johansson, K.H., 2022. Impact of Network Topology on the Resilience of Vehicle Platoons. *IEEE Transactions on Intelligent Transportation Systems*.
- POPEO, P., 2020. Federal communications commission .
- Ruan, T., Wang, H., Zhou, L., Zhang, Y., Dong, C., Zuo, Z., 2022. Impacts of Information Flow Topology on Traffic Dynamics of CAV-MV Heterogeneous Flow. *IEEE Transactions on Intelligent Transportation Systems*, 1–16doi:10.1109/TITS.2022.3170965.

- Ruan, T., Zhou, L., Wang, H., 2021. Stability of heterogeneous traffic considering impacts of platoon management with multiple time delays. *Physica A: Statistical Mechanics and its Applications* 583, 126294.
- Sala, M., Soriguera, F., 2021. Capacity of a freeway lane with platoons of autonomous vehicles mixed with regular traffic. *Transportation research part B: methodological* 147, 116–131. Publisher: Elsevier.
- Saravanan, S., Syed Ali, M., Rajchakit, G., Hammachukiattikul, B., Priya, B., Thakur, G.K., 2021. Finite-time stability analysis of switched genetic regulatory networks with time-varying delays via Wirtinger's integral inequality. *Complexity* 2021. Publisher: Hindawi.
- Schrank, D., Eisele, B., Lomax, T., 2019. Urban mobility report 2019 Publisher: Texas Transportation Institute.
- Sun, J., Zheng, Z., Sun, J., 2018. Stability analysis methods and their applicability to car-following models in conventional and connected environments. *Transportation research part B: methodological* 109, 212–237. Publisher: Elsevier.
- Suresh, R., Manivannan, A., 2021. Robust stability analysis of delayed stochastic neural networks via Wirtinger-based integral inequality. *Neural Computation* 33, 227–243. Publisher: MIT Press One Rogers Street, Cambridge, MA 02142-1209, USA journals.info
- Verizon North, L.L.C., 2020. Federal Communications Commission. Proceeding Number 19, 354.
- Vu, H.V., Liu, Z., Nguyen, D.H.N., Morawski, R., Le-Ngoc, T., 2020. Multi-agent reinforcement learning for joint channel assignment and power allocation in platoon-based C-V2X systems. *arXiv preprint arXiv:2011.04555*.
- Vukadinovic, V., Bakowski, K., Marsch, P., Garcia, I.D., Xu, H., Sybis, M., Sroka, P., Wesolowski, K., Lister, D., Thibault, I., 2018. 3GPP C-V2X and IEEE 802.11p for Vehicle-to-Vehicle communications in highway platooning scenarios. *Ad Hoc Networks* 74, 17–29. doi:10.1016/j.adhoc.2018.03.004.
- Wang, M., 2018. Infrastructure assisted adaptive driving to stabilise heterogeneous vehicle strings. *Transportation Research Part C: Emerging Technologies* 91, 276–295. URL: <https://doi.org/10.1016/j.trc.2018.04.010>, doi:10.1016/j.trc.2018.04.010. publisher: Elsevier.
- Wang, M., Hoogendoorn, S.P., Daamen, W., van Arem, B., Shyrokau, B., Happee, R., 2018. Delay-compensating strategy to enhance string stability of adaptive cruise controlled vehicles. *Transportmetrica B* 6, 211–229. URL: <https://doi.org/10.1080/21680566.2016.1266973>, doi:10.1080/21680566.2016.1266973.
- Wang, Y., Xia, Y., Zhou, P., 2016. Fuzzy-model-based sampled-data control of chaotic systems: A fuzzy time-dependent lyapunov-krasovskii functional approach. *IEEE Transactions on fuzzy systems* 25, 1672–1684.
- Wilson, R.E., 2008. Mechanisms for spatio-temporal pattern formation in highway traffic models. *Philosophical Transactions of the Royal Society A: Mathematical, Physical and Engineering Sciences* 366, 2017–2032. Publisher: The Royal Society London.
- Wilson, R.E., Ward, J.A., 2011. Car-following models: Fifty years of linear stability analysis - a mathematical perspective. *Transportation Planning and Technology* 34, 3–18. doi:10.1080/03081060.2011.530826.
- Xiao, L., Wang, M., Schakel, W., van Arem, B., 2018. Unravelling effects of cooperative adaptive cruise control deactivation on traffic flow characteristics at merging bottlenecks. *Transportation research part C: emerging technologies* 96, 380–397.
- Ye, L., Yamamoto, T., 2018. Impact of dedicated lanes for connected and autonomous vehicle on traffic flow throughput. *Physica A: Statistical Mechanics and its Applications* 512, 588–597.
- Yu, W., Hua, X., Wang, W., 2021. Investigating the longitudinal impact of cooperative adaptive cruise control vehicle degradation under communication interruption. *IEEE Intelligent Transportation Systems Magazine* .
- Zhang, C.K., He, Y., Jiang, L., Wu, M., Zeng, H.B., 2016. Stability analysis of systems with time-varying delay via relaxed integral inequalities. *Systems & Control Letters* 92, 52–61. Publisher: Elsevier.
- Zhang, X., Jarrett, D.F., 1997. Stability analysis of the classical car-following model. *Transportation Research Part B: Methodological* 31, 441–462.
- Zheng, Y., Li, S.E., Li, K., Wang, L.Y., 2015a. Stability margin improvement of vehicular platoon considering undirected topology and asymmetric control. *IEEE Transactions on Control Systems Technology* 24, 1253–1265. Publisher: IEEE.
- Zheng, Y., Li, S.E., Wang, J., Cao, D., Li, K., 2015b. Stability and scalability of homogeneous vehicular platoon: Study on the influence of information flow topologies. *IEEE Transactions on intelligent transportation systems* 17, 14–26.
- Zhong, Z., Lee, E.E., Nejad, M., Lee, J., 2020. Influence of CAV clustering strategies on mixed traffic flow characteristics: An analysis of vehicle trajectory data. *Transportation Research Part C: Emerging Technologies* 115, 102611.
- Zhou, L., Ruan, T., Ma, K., Dong, C., Wang, H., 2021. Impact of CAV platoon management on traffic flow considering degradation of control mode. *Physica A: Statistical Mechanics and its Applications* 581, 126193.
- Zhou, Y., Ahn, S., Wang, M., Hoogendoorn, S., 2020. Stabilizing mixed vehicular platoons with connected automated vehicles: An H-infinity approach. *Transportation Research Part B: Methodological* 132, 152–170.
- Zhou, Y., Wang, M., Ahn, S., 2019. Distributed model predictive control approach for cooperative car-following with guaranteed local and string stability. *Transportation research part B: methodological* 128, 69–86.